

ACCEPTED MANUSCRIPT

Silicon-based soft parallel robots 4D printing and multiphysics analysis

To cite this article before publication: Ali Zolfagharian *et al* 2022 *Smart Mater. Struct.* in press <https://doi.org/10.1088/1361-665X/ac976c>

Manuscript version: Accepted Manuscript

Accepted Manuscript is “the version of the article accepted for publication including all changes made as a result of the peer review process, and which may also include the addition to the article by IOP Publishing of a header, an article ID, a cover sheet and/or an ‘Accepted Manuscript’ watermark, but excluding any other editing, typesetting or other changes made by IOP Publishing and/or its licensors”

This Accepted Manuscript is © 2022 IOP Publishing Ltd.

During the embargo period (the 12 month period from the publication of the Version of Record of this article), the Accepted Manuscript is fully protected by copyright and cannot be reused or reposted elsewhere. As the Version of Record of this article is going to be / has been published on a subscription basis, this Accepted Manuscript is available for reuse under a CC BY-NC-ND 3.0 licence after the 12 month embargo period.

After the embargo period, everyone is permitted to use copy and redistribute this article for non-commercial purposes only, provided that they adhere to all the terms of the licence <https://creativecommons.org/licenses/by-nc-nd/3.0>

Although reasonable endeavours have been taken to obtain all necessary permissions from third parties to include their copyrighted content within this article, their full citation and copyright line may not be present in this Accepted Manuscript version. Before using any content from this article, please refer to the Version of Record on IOPscience once published for full citation and copyright details, as permissions will likely be required. All third party content is fully copyright protected, unless specifically stated otherwise in the figure caption in the Version of Record.

View the [article online](#) for updates and enhancements.

Silicon-Based Soft Parallel Robots 4D Printing and Multiphysics Analysis

Ali Zolfagharian^{1*}, Saleh Gharai¹, Abbas Z. Kouzani¹, Mohammad Lakhi², Sadegh Ranjbar², Mohammadreza Lalegani Dezaki³, Mahdi Bodaghi³

¹School of Engineering, Deakin University, Geelong, Victoria 3216 Australia

²Department of Mechanical Engineering, Birjand University of Technology, Birjand, Iran

³Department of Engineering, School of Science and Technology, Nottingham Trent University, Nottingham NG11 8NS, UK

*Corresponding author's email address: a.zolfagharian@deakin.edu.au

Abstract

Four-dimensional (4D) printing has set the stage for a new generation of soft robotics. The applications of rigid planar parallel robotic manipulators are also significant because of their various desirable characteristics, such as lower inertia, higher payload, and high accuracy. However, rigid planar parallel robots are heavy and require different actuators and components. This study introduces a novel technique to produce a light three degrees of freedom (DOF) soft parallel manipulator at a low cost, which can be stimulated easily. This technique allows researchers to customize the actuator's design based on the requirement. The robot is made by 3D printing based on fused deposition modelling (FDM) and a direct ink writing (DIW) process. The design, development, and additive manufacturing (AM) of a soft parallel robot electrothermally driven by a linear silicon-based actuator and polylactic acid (PLA) parts are presented. Silicon-based soft actuators replace the rigid conventional linear actuators in this study to drive the planar parallel manipulator. The actuation of actuators is conducted using simple heating compared to the conventional rigid actuator. Various heating approaches and configurations are compared and analysed to find the most suitable one for the effective linear stroke of the soft actuator. The finite element model (FEM) is used to analyse the performance of the electrothermally silicon-ethanol soft actuators in ABAQUS. The kinematics of the planar parallel robotic manipulator are simulated in MATLAB to achieve its workspace. The final soft parallel robot mechanism and the active and passive links are fabricated and tested experimentally.

Keywords: Silicon; 3D printing; robotic materials; soft parallel robots; 4D printing

1. Introduction

Soft robotics is an emerging field of robotics that uses a unique approach to develop low-cost multi degrees of freedom (DOF) actuators. These robots employ soft materials, such as silicon rubber and hydrogels [1]. As compared to conventional robotic actuators, soft robots have advantages such as flexibility, replicating biological systems, and high dexterity in confined spaces. These allow them to be used in various applications, such as invasive surgeries [2], handling fragile objects, and movement in rough terrains [3]. It requires considerable time and effort to produce them using traditional techniques, such as micro-molding, solid freeform fabrication, and mask lithography [4-7]. The current strategy is to create soft robots in a single step using additive manufacturing (AM) technology [8], which reduces labour and cost requirements while allowing for intricate designs and customisation. [9, 10].

Various soft robotic actuation techniques have been developed by the researchers, which include pneumatic and hydraulic [11, 12], electroactive polymers [13], shape memory alloys [14], and shape memory polymers [15, 16]. Nevertheless, these methods have certain shortcomings. For instance, the high voltage is required to stimulate electroactive polymer, the minimal strain produced by shape memory alloys, and the need for external compressors and pressure-regulating equipment for hydraulic and pneumatic systems [17]. Phase change material elastomer composite (PCMEC) actuators are a type of thermally actuated soft material that uses phase shift in each section of the phase change fluid to cause macroscopic expansion used to actuate soft robots [18, 19]. Compared to the traditional electromechanical ways, they offer a promising solution to the difficulty of activating soft robotic materials.

One such PCMEC is the PDMS-based silicon elastomer as the matrix material and ethanol as the active fluid [17, 20, 21]. Miriyev et al. were successfully able to fabricate and test the functioning of one such silicon elastomer and ethanol actuator [17]. Xia et al. tried to overcome the low thermal conductivity of silicon rubber, which hinders the uniform heating of the material, with the addition of diamond nanoparticle-based thermally conductive fillers [20]. Li et al. compared silicon actuators with various actuating fluids such as water and ethanol. It was observed that these actuators were robust and suitable for the fabrication of soft actuators [22]. Several methods of actuating soft thermal silicon actuators have been presented in the literature. Cartolano et al. utilised highly flexible conductive fabric heaters for soft thermal actuators. Furthermore, the use of various kirigami shapes allowed them to achieve specific motions [21]. Infrared radiation (IR) was also successfully explored as the untethered stimuli to produce the required activation in the soft actuators [23, 24]. Miriyev et al. have efficiently used a high-resistance nichrome metal wire coiled up in a spiral shape, like a spring, to develop an electrically actuated soft thermal actuator that uses a DC power supply. This actuator is found to be robust, straightforward to fabricate, limited with tethered connection [17].

Parallel robotic mechanisms introduce several advantages, such as low inertial disturbances and high precision control [25, 26] compared to their serial counterparts. Micro positioning where small but exact movements are primary objectives is used in numerous applications including cars, cameras, telescopes, scanning electron microscope (SEM), atomic force microscope (AFM), and semiconductor manufacturing [27]. Planar parallel mechanisms are generally used in a wide range of micro-positioning applications [28] while are characterized

1
2
3 by their end effectors ability to generate planar motions. One of the popular families of 3-DOF
4 planar parallel manipulators is the three-prismatic-revolute-revolute (3-PRR) mechanism,
5 which consists of a single prismatic joint and two revolute joints. The 3-PRR mechanism is a
6 special type of symmetrical planar mechanism that has three kinematic chains with the identical
7 topology that all connect the fixed base to the moving platform [29]. For the successful
8 functioning of the 3-PRR mechanism, the soft actuator must be able to produce linear actuation.
9 One effective approach is by using asymmetries in the design of the soft actuators to produce
10 linear motion [30].

11
12
13
14 Four-dimensional (4D) printing of PCMEC into soft parallel robot applications is introduced,
15 which is a novel technique to develop soft 3-PRR manipulators instead of rigid manipulators.
16 Utilising the AM of tethered linear soft actuators that are specifically suited to a 3-PRR
17 manipulator is used in this study. The modern approach is to use AM technology to develop
18 soft parallel manipulators, including the linear actuators, reducing labour and cost requirements
19 while enabling customization.
20
21
22

23 This work focuses on the development of a 3-PRR mechanism using a thermally actuated
24 silicon-based soft actuator. The actuators can be easily stimulated by an electro-heating system.
25 This technique allows researchers to customise the actuator's design based on requirements.
26 Various approaches to heating the silicon-based actuators are compared and analysed to find
27 the most suitable approach and configuration to produce a suitable expansion for the linear
28 actuation. The actuators and mechanism designs are modelled first using finite element analysis
29 in ABAQUS and kinematic simulation in MATLAB. The nonlinearities and complex
30 geometries of soft actuators prevent the development of analytical models to describe their
31 motion. Finite element modeling (FEM) provides an effective solution to this issue and allows
32 the user to predict a more realistic performance of the system's nonlinear response via
33 commercially available software packages such as ABAQUS. Implementation of FEM in the
34 design process of soft actuators with 3D printing helps with accurately predicting behavior and
35 optimizing the performance and topology, which leads to a better understanding of the effect
36 of geometric parameters, stimulus, and material selection on the performance of the robots.
37 Numerical and experimental results showed that this method is very effective for the fast and
38 efficient design of soft actuators to meet specific design requirements and save time and design
39 resources in soft robot manufacturing. Then, the final soft parallel robot mechanism and the
40 active and passive links are printed and tested experimentally.
41
42
43
44
45
46
47
48
49

50 **2. Methodology**

51 This work has been carried out in different stages, namely the materials preparation and
52 manufacturing of silicon-based linear soft actuators, and polylactic acid (PLA)-based parts; the
53 forward kinematic, inverse kinematics, and workspace simulation of the 3-PRR planar
54 mechanism using MATLAB software; finite element analysis (FEA) of the electrothermal
55 actuators, and the experimental analysis of the developed robotic mechanism model using
56 linear soft actuators and PLA-based mechanism.
57
58
59
60

2.1. Materials preparation and manufacturing

The 3-DOF U-shape planar parallel robotic manipulator is modelled in Solidworks software. The design is converted into standard tessellation language (STL) format for 3D printing as shown in Fig. 1(A). Also, fused deposition modelling (FDM) is employed for the rapid fabrication of 3D CAD models. The passive robotics parts and joints are fabricated in Flash Forge Creator 3 3D printer using PLA material. The linear soft actuators are made of silicon-ethanol composite as illustrated in Figs. 1(A) and 1(B) and served as prismatic joints to the mechanism. The silicon-based soft actuator is fabricated as per earlier receipt [31] of the thermal responsive soft actuators. The precursors of Ecoflex™ 00-50, Part A and Part B (Smooth-On, Inc.) are first mixed with ethanol (98%). A mixture of Ecoflex-00-50 from Smooth-on silicon rubber as the matrix material and a 20% volume of ethanol as the active material. For the silicon elastomer, 5 vol.% platinum silicon cure accelerator (Plat-Cat, Smooth-On, Macungie, PA) and 1.1 vol.% silicon thickening agent (THI-VEX, Smooth-On, Macungie, PA) are added with silicon part A. Furthermore, 20 g of Ecoflex-00-50-part A is mixed with 10 ml of ethanol using a plastic spatula and loaded into syringe A. Furthermore, 20 g of Ecoflex-00-50-part B is loaded into syringe B. Then, the syringes are loaded into the syringe pumps. The syringes are heated in the nozzle before being extruded, by a BIO X™ - 3D bioprinter - CELLINK, into a mould designated for holding the heater. The extruded ink in the mould is left at room temperature to be cured for 3 hours according to the procedure used in [17, 31]. The materials and their properties used in this study process are presented in Table 1.

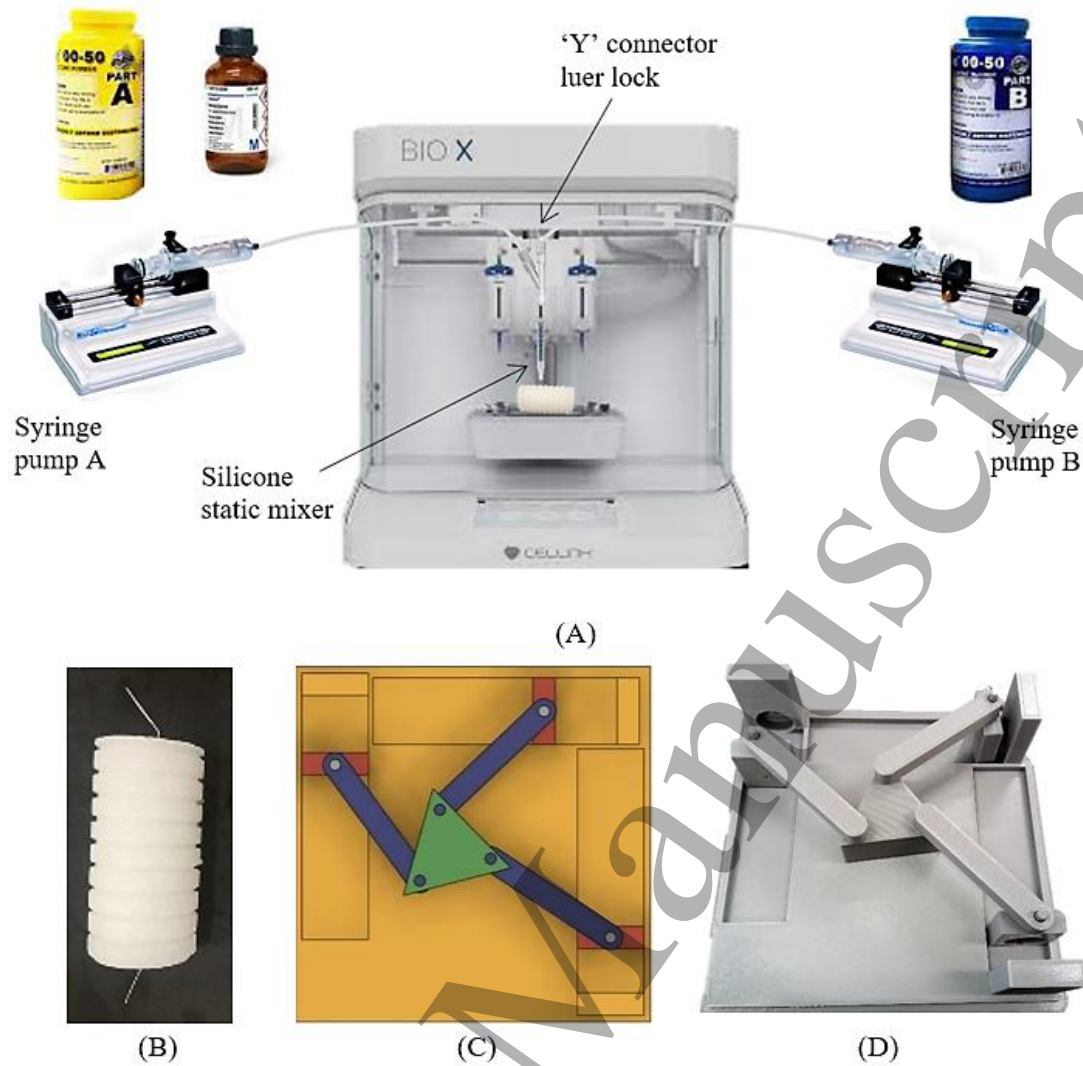


Fig. 1. (A) 3D printer set up and Ecoflex™ 00-50 materials (B) silicon-ethanol soft actuator (C) CAD model and (D) FDM 3D-printed 3-PRR manipulator.

Table 1. Properties of materials used for the actuators.

Material	Properties								
	Density (Kg/m ³)	Young's modulus (MPa)	Poisson's ratio	Thermal expansion coefficient (K ⁻¹)	Thermal conductivity (W/m.K)	Specific heat units (JM ⁻¹ θ ⁻¹)	Elongation at break (%)	Mixed viscosity (cps)	Tensile strength (psi)
Silicon	1100	52000	0.45	0.0025	0.4	1.9	-	-	-
Ecoflexin+ Ethanol									
Nichrome wire	7750	15000	0.26	9	8	0.38	-	-	-
Polyamide tape	1420	2500	0.34	20	0.120	1.09	-	-	-
Ecoflex 00-50	1070	-	-	-	-	-	980	8000	315

2.2. Kinematics analysis of the 3-PRR robot

The feasibility of the 3-PRR planar mechanism is analysed using MATLAB software. A mathematical relationship between the end effectors and the specified values of the joint parameters is analysed using kinematics analysis. Forward kinematic analysis helps to predict the position of the end effector for given joint parameters. On the other hand, inverse kinematic analysis helps to predict the positions of joint parameters from the given position of the end effector. The first joint at each limb of the 3-DOF planar parallel manipulator is considered to be an active prismatic joint (P) because of its multiple advantages, such as modular design, back drivability, compactness, reduction in link interferences, large singularity-free workspace, simple kinematic arrangement, ease of control, and low inertial properties of the moving system [32, 33]. Every limb of this planar parallel manipulator begins with an active prismatic joint followed by passive joints and links that connects fixed base to the end-effector.

The three soft actuators are represented as three cylindrical mechanisms for ease of implementation and kinematic analysis. The diagrammatic representation of the end effector of the PRR mechanism and the correlation between the active translational joint and the pose of the end-effector are shown in Fig. 2. All the active controllable inputs are considered as active prismatic (translational) inputs for the design and analysis. The PRR manipulator has three limbs—one along the X-axis and the other two along the Y-axis. The limb along the X-axis is referred to as limb-1, the left limb along the Y-axis is referred to as limb-2, and the right limb along the Y-axis is referred as limb-3. Each limb consists of an electrothermal soft silicon actuator for bidirectional actuation and serves as an active prismatic joint or the joint space displacement (r_1 , r_2 and r_3).

The shape of the end-effector considered is an equilateral triangle of side length 'a' and height 'h' connected to the fixed U-shape base platform by three limbs. Active joint displacements, namely as three soft actuators, are denoted by ' r_i ' ($i = 1,2,3$) as shown graphically in Fig. 2. The link length of the connecting members connecting the active prismatic joint and the end-effector is denoted by ' l_j ' ($j = 2,4,6$). 's' and 'h' are the width and height of the fixed U-shape base, respectively. The orientation (rotation about the z-axis) of the mobile platform is denoted by ' θ '. The angles of each of the prismatic joints made with the connecting rods are marked as θ_i ($i = 2,4,6$). Forward and inverse kinematics have been simulated in MATLAB as per the following equations [33].

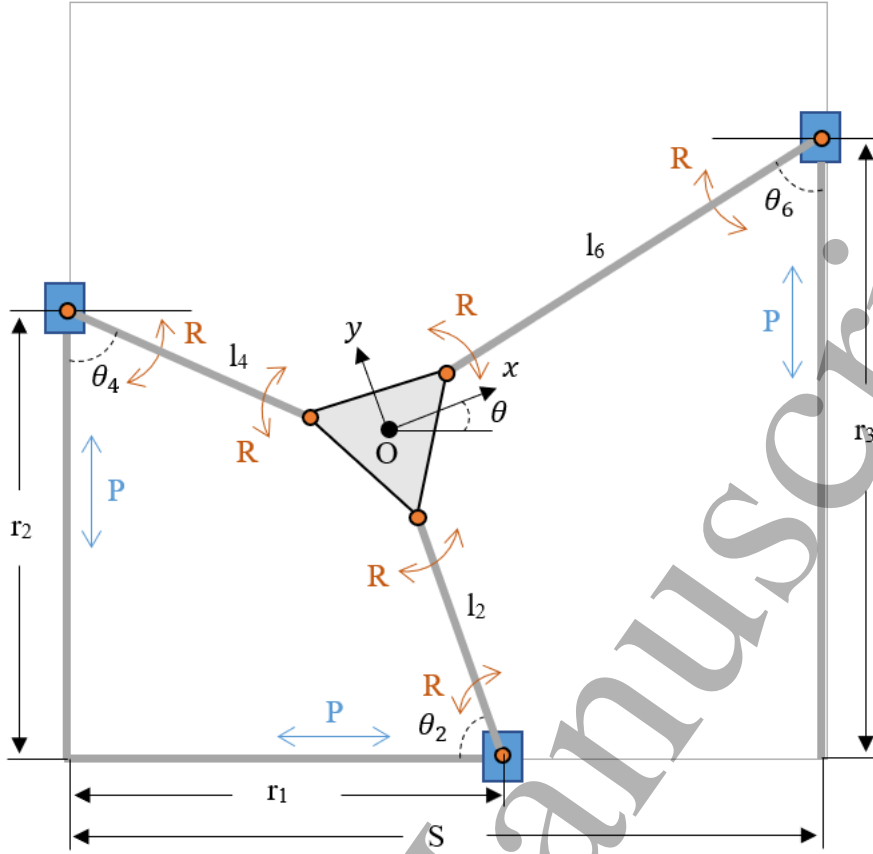


Fig. 2. The schematic representation of the PRR planar parallel manipulator.

$$\begin{aligned}
 r_1 &= x + \frac{2h}{3} \sin \theta + \gamma_1, \gamma_1 = l_2 \cos \theta_2, \theta_2 = \sin^{-1} \left(\frac{y - \frac{2h}{3} \cos \theta}{l_2} \right) \\
 r_2 &= x + \frac{2h}{3} \sin(30^\circ - \theta) + \gamma_2, \gamma_2 = l_4 \cos \theta_4, \theta_4 = \cos^{-1} \left(\frac{x - \frac{2h}{3} \cos(30^\circ - \theta)}{l_4} \right) \\
 r_3 &= y + \frac{2h}{3} \sin(30^\circ + \theta) + \gamma_3, \gamma_3 = l_6 \cos \theta_6, \theta_6 = \cos^{-1} \left(\frac{s - x - \frac{2h}{3} \cos(30^\circ + \theta)}{l_6} \right)
 \end{aligned} \tag{1}$$

Jacobian matrix (J) refers to the velocity transformation/mapping matrix which maps the Cartesian space velocities to the joint space velocities in the planar parallel manipulator. The Jacobian matrix for the PRR fixed base manipulator is calculated as follows.

$$J = \begin{bmatrix} 1 & -\delta_1 & \delta_2 \\ -\delta_3 & 1 & \delta_4 \\ 0 & 1 & \delta_1 \end{bmatrix}$$

$$\delta_1 = -\frac{h}{3} \sin \theta + \frac{a}{2} \cos \theta, \delta_2 = \frac{2h}{3} \cos \theta - \delta_1 \frac{2h}{3} \sin \theta$$

$$\delta_3 = \frac{\sin \theta_4}{\sqrt{l_4^2 - \sin^2 \theta_4}}, \delta_4 = -\frac{2h}{3} \cos(30^\circ - \theta) - \delta_3 \frac{2h}{3} \sin(30^\circ - \theta) \quad (2)$$

Here, the side of the equilateral triangle is taken as 50mm, the length of the connecting rod is taken as 60mm, and the frame gap is taken as 120mm.

3. Results and Discussions

3.1. Experimental tests for choice of optimal method and configuration of the heating elements

The soft actuators are made in three separate forms, including a conductive fabric heater, a NiCr wire heater wound in a zig-zag and spiral shapes. The experimental setup consists of a testing rig with a DC power supply and a camera. The actuations are further measured using MATLAB image processing (imtool) software.

The three sets of actuators are tested to check the feasibility of their potential for the 3-DOF 3-PRR mechanism. First, the flexible fabric heater is prepared using polystyrene sulfonate (PEDOT:PSS) as a thin conductive film Joule heater attached to the actuator according to [21] and connected to the DC power supply at 1.5 A and 3.5 V. The actuation is recorded using a camera, and the results are shown in Table 2. The initial and final sizes of the actuators are shown in Fig. 3(A). The results show the length of actuator increases to 55.08 mm after supplying power. Similarly, the actuator with the NiCr wire is connected to the DC power supply and the same current and voltage and the initial and final sizes of the actuators are shown in Fig. 3(B). The length increase is around 5 mm from 42.42 mm to 47.26 mm for actuator with NiCr wire. Meanwhile, the soft actuator with spiral configuration has the maximum changes from 40.80 mm to 51.62 mm after stimulating (see Fig. 3(C)). From Table 2, it is observed that the expansion created by the flexible fabric heater-based actuators is significantly lower than that produced by the NiCr wire-based actuators with repeating the tests for three times. Hence, NiCr wire is chosen as the optimal heating element for the actuators.

Also, a comparison of the heating elements of the actuators is done based on their geometry to check the effectiveness of the heater design. Two conceptual configurations of the heating element are designed and compared. NiCr wires are opted with the same resistance but with different geometric configurations to assess the efficacy of the heater. The first design is a zig-zag design, while the second design is a spiral configuration as shown in Fig. 4. These two configurations are used because they are able to distribute the heat equally all over the actuator. Hence, the expanding and shrinkage can be controlled equally. Also, the actuator has better stability compared to other configurations. The expanded actuator after stimulating can be more effectively regulated by spiral and zig-zag configuration compared to other shape. The spiral and zig-zag shape heater elements are studied by applying a DC power supply, and the initial and final sizes of the actuators are recorded using a camera as shown in Fig. 3, and Table 2. The results revealed that the spiral heating element produced significantly higher linear expansion as compared to the zig-zag wire-based heater configuration.



Fig. 3 Initial size (left) and the final size (right) of the (A) flexible fabric heater-based actuator, (B) NiCr based actuator with zig-zag configuration, (C) NiCr based actuator with spiral configuration. (The values shown on the figures are the corresponding pixels of the image processing measurements before and after actuations. The scale of the pixels is shown next to the rulers in each image separately).

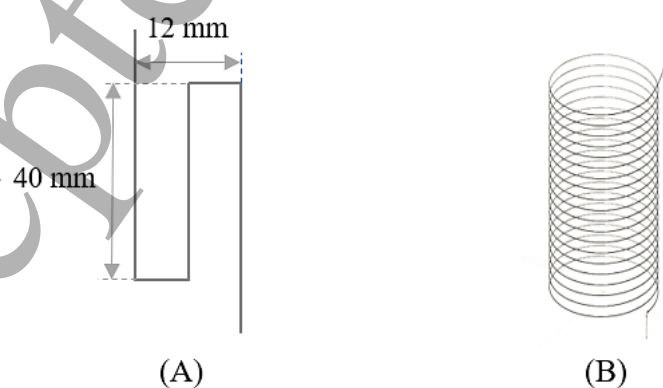


Fig. 4. The same dimensioned (A) zig-zag configuration of the NiCr wire and (B) spiral configuration of the NiCr wire.

Table 2. Actuators performance with different method and configuration of heating elements.

Type of actuators	Initial size (mm)	Final size (mm)	Actuation stroke (%)	Standard deviation (mm)
Flexible fabric	50	55.05	10.1	±0.16
NiCr (Zig-Zag)	50	56.30	12.6	±0.35
NiCr (Spiral)	50	63.20	26.4	±0.74

3.2 Design tests for asymmetry and FEA results to achieve maximum stroke

For the design of the 3-PRR mechanism, it is imperative to develop linear motion by using asymmetries for the soft actuators. Here, wrapping the polyimide tape around the soft actuators and the use of different geometries are explored to achieve maximum linear expansion. Two conceptual designs are developed, one with straight grooves over the body of the actuator and polyimide tape wrapped over it, and the other with crisscross grooves over the body and polyimide tape over it, as shown in Figs. 5 and 6. The experiment aims to ascertain the best possible design of the actuators as per the conceived designs for producing maximum linear asymmetries. The size of the straight grooved actuator before and after actuation can be seen in Fig. 3(A). Similarly, the size of the crisscross grooved actuator is compared in Fig. 3(B). The results of the expansion are shown in Table 3. From Table 3, it can be observed that a straight grooved actuator with polyimide tape wrapped over it produces a significant increase in linear expansion of 46% as compared to a criss-cross grooved actuator with polyimide tape wrapped over it. As shown in Fig. 5, The straight grooved actuator has a higher linear stroke. This is because of the equally expanded spiral wire around the soft silicon. In crisscross grooved actuator, as soon as the silicon is expanded, there are overlapped between rounded wire. This phenomenon decreases the linear stroke of the actuator because of the limitation in wire expansion. Meanwhile, the straight grooved actuator is expanded equally due to the spiral shape behaviour. As soon as the silicon is expanded, the spring-shaped wire stretches and swells. Also, the crisscross grooved actuator tends to bend instead of linear after silicon expands. That is why it is a good option for bending compared to the straight grooved actuator [34, 35].

The finite element analysis (FEA) part included a description of the developing model by applying loads, boundary conditions, and mesh assignment. As shown in Table 1, the ABAQUS software is used to model four actuators using the material properties from the previous experiments [36]. The interaction between the parts and contact types are assigned. Power is given as input in the form of loads and boundary conditions to the models. For the thermal actuators, the materials used for the parts are silicon Ecoflex 00-50 mixed with ethanol, Ni-Cr wire, and polyamide tape. The actuation process is to supply electricity to the Ni-Cr wire from both ends, which will produce heat inside the actuator. This eventually leads to the expansion of the actuator.

This happens when ethanol reaches the liquid-gas transition temperature, which is contained inside tiny microbubbles embedded in the elastic silicon rubber matrix, it boils, causing a considerable volume rise and significant expansion of the entire soft composite material. Ethanol is disseminated in bubble-shaped pores throughout the silicon elastomer matrix as a result of mixing, where it combines with its vapours to create a localised pressure equilibrium. The process of curing involves ethanol vapours occupying air pockets present throughout the material, forming new pores, and decreasing the developing internal vapour pressure by widening the pores until the material's internal and external vapour pressures are equal. Temperature-dependent ethanol liquid evaporation creates internal pressure within the bubbles, which causes the silicon elastomer matrix to gently expand. The silicon elastomer matrix significantly expands as ethanol passes the liquid-to-vapor phase transition, causing an extraordinary volume change [37]. This volume change in soft actuator is controlled by spiral and zig-zag configuration which lead to uniform actuating system.

To simulate the same in ABAQUS, coupled temperature-displacement analysis is considered the best option. The required properties to analyse the expansion using temp-displacement fit the earlier work by Kapłan and Milecki [36]. This model is developed to increase the linear expansion of the actuator by restricting the radial expansion of the actuator. Grooves are given to the actuator, and polyamide tape bands are wrapped in the grooves to restrict the motion, and the rest is similar to a simple spiral heater actuator. This actuator has three basic parts: silicon actuator with grooves, coiled Ni-Cr wire, and polyamide tape bands. The wire is embedded into the actuator model in such a way that the two ends of the Ni-Cr wire stand out from the actuator. The heat generated in the FEA simulation of simple spiral heater actuator is imported into this model to reduce the work as the wire used is the same for both actuators. The contact between the actuator and Ni-chrome wire is a TIE, whereas the contact between the actuator and polyamide tape is a frictional contact. These parts are also considered to have thermal and mechanical contacts. The element used to simulate C3D4T is intended. The displacement contour of simulation results for different actuators is demonstrated in Fig. 5. Also, the linear displacement versus time diagram of actuators with different heating element configurations and asymmetries is shown in Fig. 7 in comparison with experimental results.

Table 3. Asymmetry produced by various designs with polyimide tape.

Type of actuators	Initial size (mm)	Final size (mm)	Actuation stroke (%)	Standard deviation (mm)
Straight grooved	50	72.9	45.8	±2.12
Crisscross grooved	50	65.1	30.2	±1.84

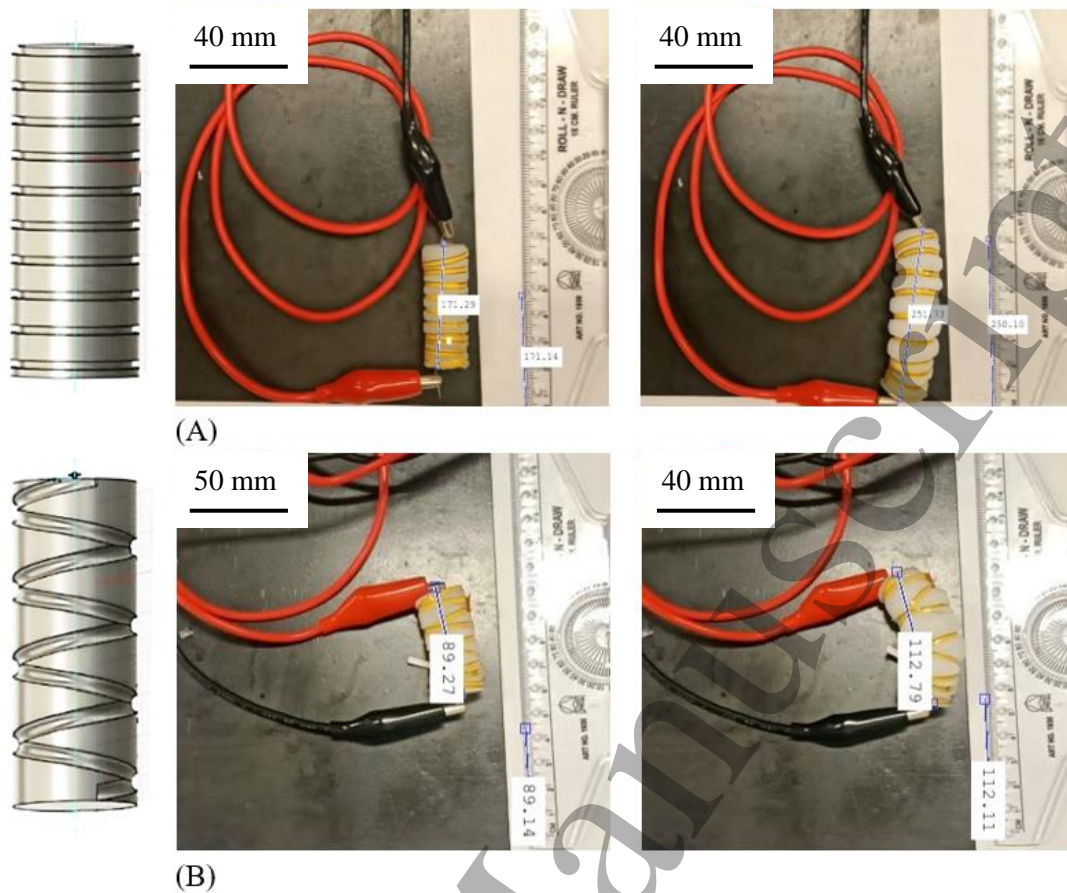


Fig. 5. Initial size (left) and the final size of the (a) straight grooved actuator with polyimide tape actuator (b) crisscross grooved actuator with polyimide tape.

3.3. Soft parallel robot kinematic results

These silicon-based soft actuators are attached to a real 3-PRR U-shape planar mechanism, which is then tested for functionality. A MATLAB model of the forward kinematics, inverse kinematics, and workspace of the newly created 3-DOF U-shape planar mechanism is simulated, and a trajectory representing the actual model is completed.

Three simulations have been carried out using the maximum stroke of linear actuators of 16 mm to determine the workspaces. The workspace generated is shown in Fig. 6(A). Also, a planned trajectory in which the P2 actuator is held at 50 mm and activates P1 and P3 such that they are expanded to 56 mm each is simulated as shown in Fig. 6(B). As shown in Fig. 6(C), this trajectory is further validated using experimental values of the mechanism. The parallel robot's end-effector can be seen following the simulated trajectory that is created in MATLAB, according to measurements of the end effector trajectory taken from the video.

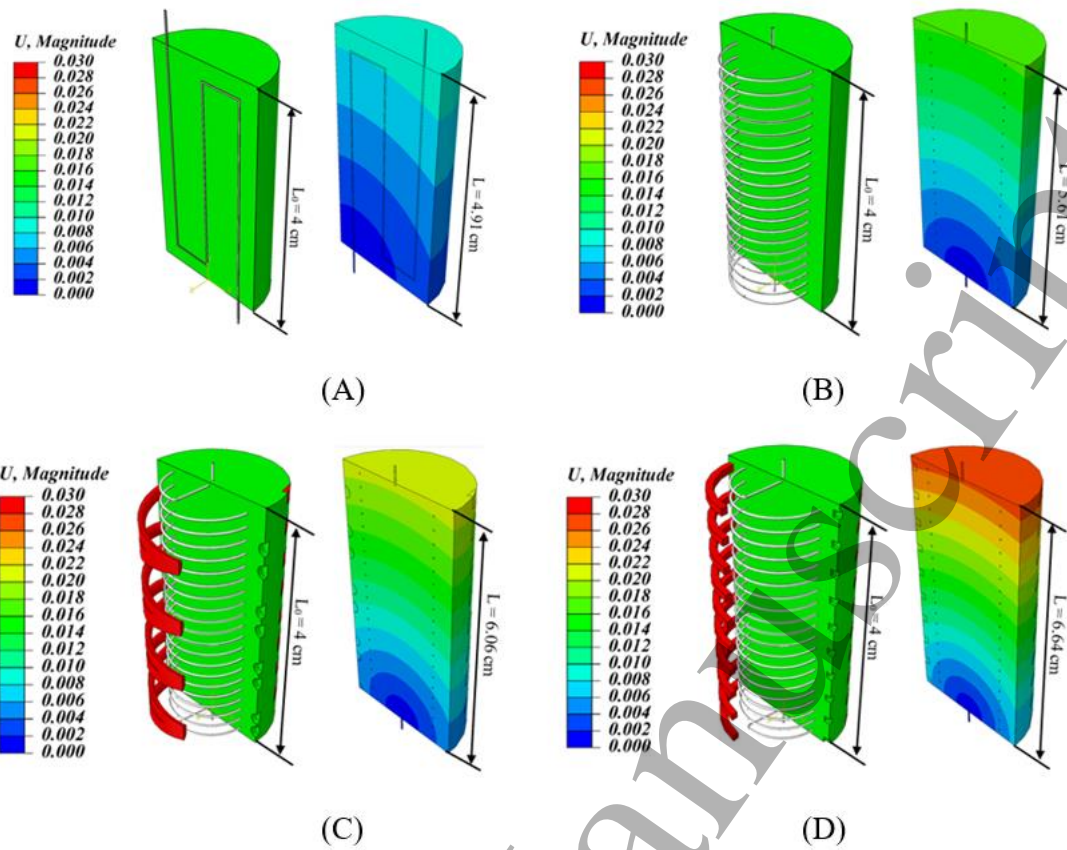


Fig. 6. Displacement Contour for different actuators before (left) and after (right) actuations, (A) Simple printed silicon actuator_Zig_Zag (B) Simple cast silicon actuator_Spiral (C) Criss cross cast silicon actuator_Spiral (D) Straight groove cast silicon actuator_Spiral.

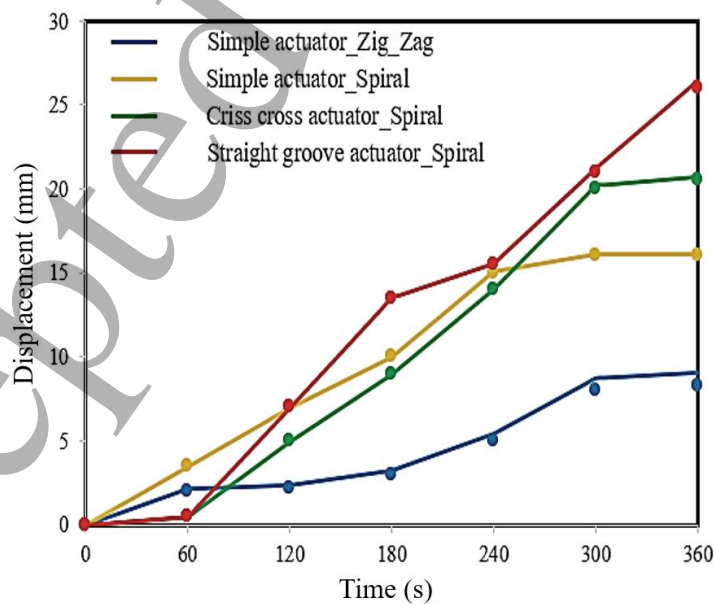


Fig. 7. Comparisons of displacement versus time for different actuators using simulation and experimental results.

The relationship between temperature and displacement is important to find out differences. The following formula is used to derive the relationship between temperature and displacement:

$$(l_f - l_o)/l_o = \alpha_l(T_f - T_0) \quad (3)$$

where, l_f is the final length of the actuators, l_o is the initial length of the actuators, α_l is the coefficient of linear thermal expansion, T_f is the final temperature and T_0 is the initial temperature. The difference between the initial and final lengths is the amount of displacement of the soft actuator, and the temperature difference over the time of heating could be measured as well. Thus, Eq. (3) can be rewritten as follows.

$$U_t/l_o = \alpha_l * T_t \quad (4)$$

where, U_t and T_t is the displacement and the temperature time-dependent, respectively. According to the materials properties, shown in Table 1, the most effective value of the expansion coefficient is related to the silicon-ethanol composite.

According to the Table 1, the value of the effective expansion coefficient is equal to 0.0025 K^{-1} . Also, the initial length of the actuator is equal to 40 mm. So:

$$U_t/40 = 0.0025 * T_t \quad (5)$$

or

$$T_t = 10U_t \quad (6)$$

Eq. (6) shows that if the T_t is applied $10U_t$ (that U_t is extracted from the experimental test), the simulation results and the experimental results are well matched (as illustrated in Fig. 7)

The presence of DC current of 1.5 A and a potential voltage of 3.5 v in NiCr wires inside the zig-zag and spiral heater actuators causes different amounts of heat, leading to different thermal gradients in each of the two types of wires. Also, experimental results show that the actuator, including the spiral spring, has a higher temperature than the zig-zag spring, which causes this actuator to have more displacement. Fig. 8 shows the temperature-time behaviour for each of the heaters. According to this figure and spring geometry, the spiral spring can create a temperature that is more than twice the temperature of the zig-zag spring after 6 minutes. In other words, according to the linear relationship between temperature and displacement, it causes the actuator displacement to increase more than twice.

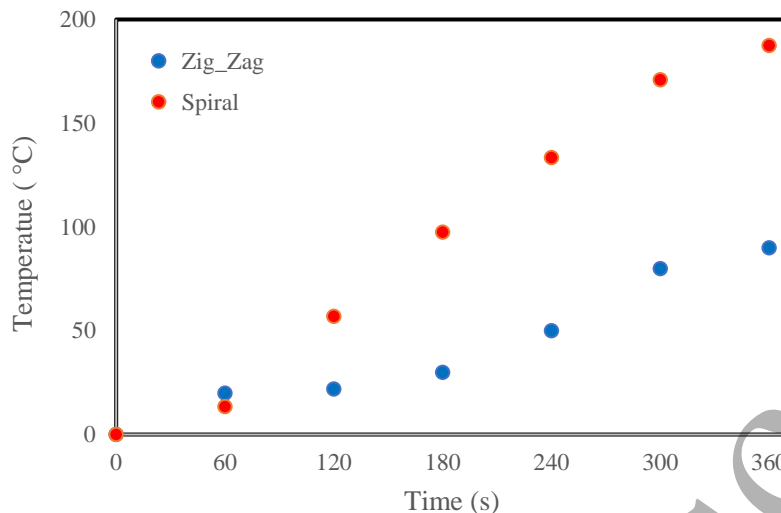


Fig. 8. The results of temperature-time behaviour for each of the heaters.

The comparison of the simulation and experimental results of the soft actuators in the 3-PRR parallel manipulator reveals that the ideal workspace area is greater as compared to the feasible workspace area. Fig. 6(A) depicts the loss incurred in the manipulator due to the difference in maximum contraction length between the ideal and the feasible condition. The loss incurred is due to the displacements along individual axes, which in turn leads to a reduction in the workspace area of the manipulators.

Having developed and demonstrated the 4D printing concept application in soft parallel robot development using silicon-based actuators shows the technique is able to be used instead of rigid manipulators. It is seen that there is a bend in the crisscross grooved actuator. Based on the FEA and experimental results, each of the crisscross grooved actuator and the straight grooved actuator provided a considerable amount of expansion, but the only difference is that the straight grooved expansion provided linear expansion and the crisscross grooved actuator has a bend in it along with linear expansion.

The constructed model has several link joints that interface with different modules or components. When the input prismatic joint is actuated, the motion is conveyed through the different linkages and joints that connect the end-effector to the input translational joints. As the links and joints move relative to one another, the relative force and velocity of the links and joints decrease due to the friction. Because of the loss of relative forces and velocity, the stroke length of the input translational joints and end-effector motion is reduced, resulting in a reduction in the manipulators' total workspace. Figs. 9(A) and 9(B) show the results of trajectory path of 3-PRR using MATLAB. The results indicate the mechanism work properly in terms of moving the joint and end effectors (see Fig. 9(C)).

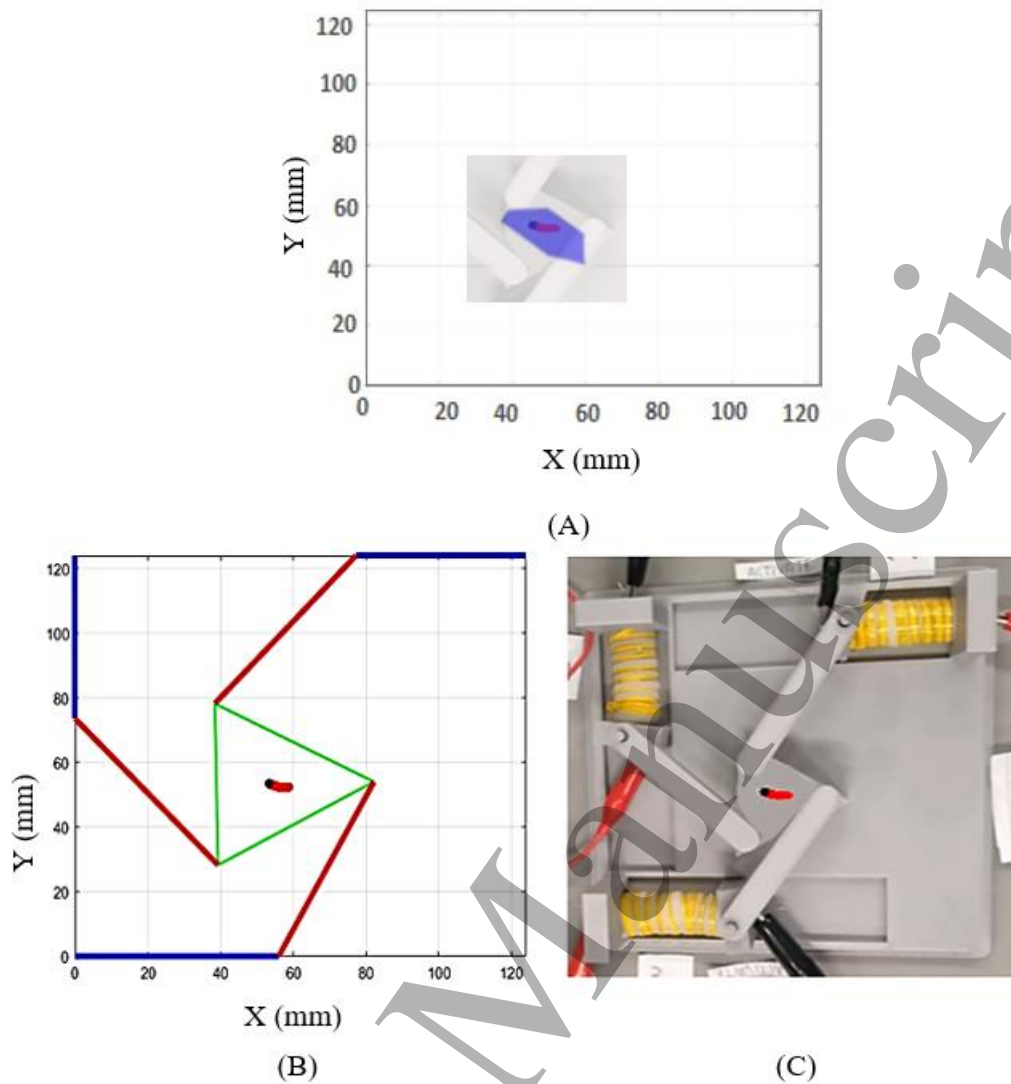


Fig. 9. (A) Workspace of the 3-PRR robot shaded blue (B) Trajectory of the end effector in the simulation and (C) experimental tests with the straight grooved actuators.

The trials demonstrate that the soft actuators are consistently able to autonomously stimulate the system inside its workspace, organise the arm motions, and carry out the task of moving the object. The available workspace and the maximum payload must be balanced. However, by increasing the length of soft actuators, it is possible to increase the maximum distance. Greater workspace can be reached while less payload can be moved as the arm's length extends. It is determined that the entire trajectory needed to be smoothed out with a number of intermediate waypoints. One arm segment's length affects how many intermediate waypoints there are. The Y position error of each actuator is investigated after three runs.

Fig. 10(A) shows the procedure of error points for each actuator. Figs. 10(B) illustrates the average errors after stimulating the soft actuators for 360 seconds. The results indicate that the actuators work well with a maximum of 1.20 mm error. Due to the soft nature of the actuators, the obtained results are reliable, but they are not as precise as rigid ones. However, the mechanism works properly with these minor errors. Measuring the precision and stability of the mechanism is conducted via reaching a target point in the middle of the mechanism at the

1
2
3 maximum length of actuators 1 and 3. The mechanism is run 50 times and the points are
4 recorded accordingly. By heating the actuators, the triangle in the middle of the mechanism
5 reaches a point. The precision and repeatability of the mechanism were recorded each time (see
6 Fig. 10(C)). The target point error is mainly between 0.3 mm and 1.5 mm in cycle tests.
7 However, the error goes higher sometimes during the test due to the actuator flexibility.
8
9

10 To compare this parallel robot with previous works, the trajectory path for the end of the
11 triangle for actuators 1 and 3 is developed in MATLAB. Fig. 10(D) shows the differences
12 between this work and previous works. The movement of actuator 2 is neglected since the path
13 trajectory of this actuator is different. The trajectory path is scaled down (0.6) to be the same
14 as in previous work to investigate the differences. The paths of actuators 1 and 3 are connected
15 to each other to show the movement of the triangle's end. By connecting the trajectory paths
16 of actuators 1 and 3, it reveals that the robot works properly. However, the movement of
17 actuator 2 for reverse movement is removed since the machine works differently from rigid
18 parallel robots. The results show the promising repeatability of the mechanism, which is close
19 to the previous work in the literature [38, 39].
20
21
22
23

24 The similarities between this robot and previous ones are due to the end effector movements.
25 In all parallel robots, there are actuators that stimulate the robot to move end effectors. In rigid
26 robots, the stepper motor and assembly of rigid components move the robot, while in this robot,
27 the soft actuators do the task. The differences between this 4D-printed robot and previous ones
28 are the actuators, which are soft in this work. Controlling soft actuators are difficult compared
29 to rigid manipulators and stepper motors. The trajectory path of actuators 1 and 3 shows the
30 machine is accurate. The target error indicates the mechanism has reliable accuracy compared
31 to rigid ones while the actuators are soft. It should be noted that the controllability and holding
32 of soft actuators in a position is more difficult than rigid counterparts.
33
34
35
36

37 Soft robotic heaters could be used in future studies. By increasing the heat conductivity of the
38 silicon elastomer using high-thermal conductivity additives such as graphene or metal particles,
39 the heating and cooling periods for future research may be reduced while keeping the expansion
40 capabilities. Also, the dynamic modelling of the presented soft parallel robot and experimental
41 studies could be conducted.
42
43
44
45
46
47
48
49
50
51
52
53
54
55
56
57
58
59
60

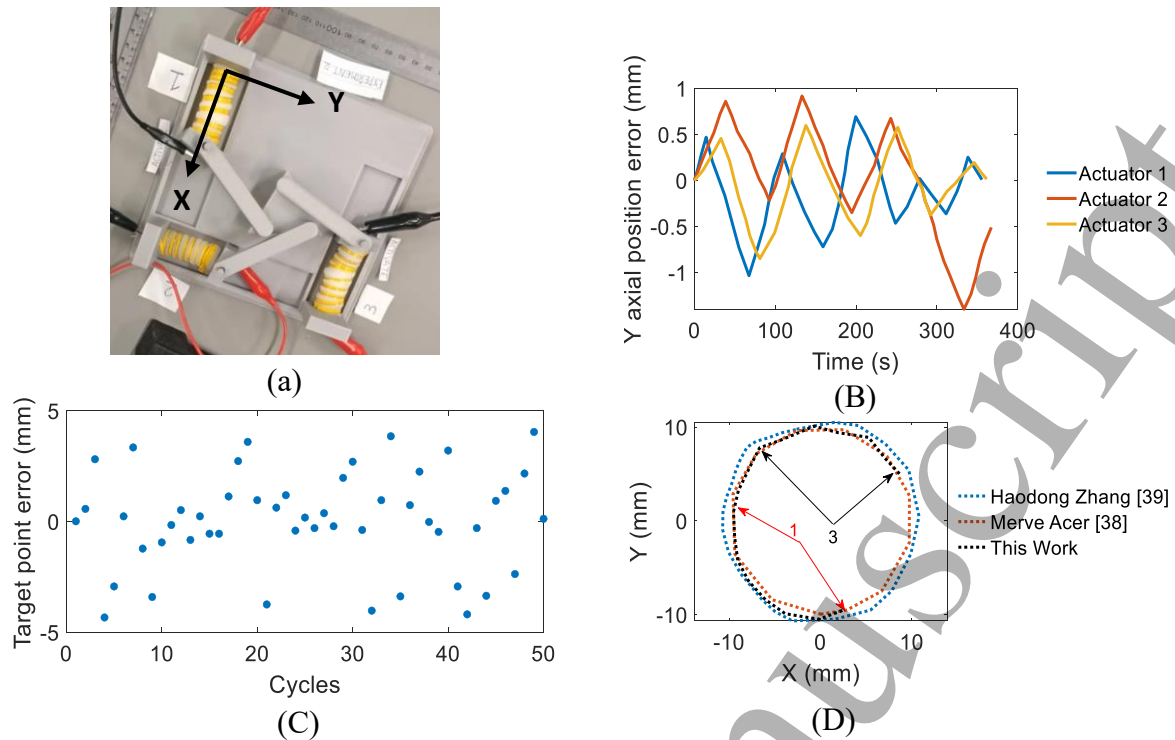


Fig. 10. (A) The position of X and Y direction for each actuator. (B) Average position error of each actuator in Y direction. (C) Target point error of mechanism in 50 cycles. (D) Trajectory path of parallel robot compared to previous works (The trajectory path of actuator 3 is black and actuator 1 is red)

4. Conclusion

An electrothermally responsive silicon-based soft parallel robot was built using 4D printing technology in this study. The soft parallel manipulator was made of a thermally responsive silicon-ethanol composite. Different electrothermally approaches, using conductive fabric and two NiCr wire configurations, were tested to find the optimum configuration to achieve the maximum expansion of the soft actuator. Having selected the spiral NiCr as the choice of study, the polyamide tape was used to wrap around the actuator to gain the most stroke. Using the FEM validated by experimental results, it was found that the straight grooved polyamide wrapped actuator led to the largest linear stroke. The optimally designed soft parallel robot was printed by the silicon-based actuator and PLA parts using DIW and FDM processes, respectively. The method allows customized design and the use of different materials accordingly. The 3-PRR manipulator was tested experimentally according to the kinematics modelling analysis. The study presented a promising strategy for use in next generation additive manufacturing of robotics using 4D materials that can enhance customisation, flexibility, and manufacturing time and effort efficiency in various soft robotic industries.

Competing interests

The author(s) declare no competing interests.

Data availability

The datasets used and analyzed during the current study available from the corresponding author on reasonable request.

References

1. Gul, J.Z., et al., *3D printing for soft robotics—a review*. 2018. **19**(1): p. 243-262.
2. Yamamura, S. and E. Iwase, *Hybrid hinge structure with elastic hinge on self-folding of 4D printing using a fused deposition modeling 3D printer*. *Materials & Design*, 2021. **203**: p. 109605.
3. Rus, D. and M.T. Tolley, *Design, fabrication and control of soft robots*. *Nature*, 2015. **521**(7553): p. 467-475.
4. Feng, G.-H. and S.-C. Yen. *Micromanipulation tool replaceable soft actuator with gripping force enhancing and output motion converting mechanisms*. in *2015 Transducers-2015 18th International Conference on Solid-State Sensors, Actuators and Microsystems (TRANSDUCERS)*. 2015. IEEE.
5. Roche, E.T., et al., *Actuators: a bioinspired soft actuated material (Adv. Mater. 8/2014)*. 2014. **26**(8): p. 1145-1145.
6. Malone, E. and H.J.R.P.J. Lipson, *Freeform fabrication of ionomeric polymer-metal composite actuators*. 2006.
7. Kerdlapee, P., et al., *Fabrication of electrostatic MEMS microactuator based on X-ray lithography with Pb-based X-ray mask and dry-film-transfer-to-PCB process*. 2014. **20**(1): p. 127-135.
8. Ji, Q., et al., *Customized protective visors enabled by closed loop controlled 4D printing*. *Scientific reports*, 2022. **12**(1): p. 1-12.
9. Zolfagharian, A., et al., *Evolution of 3D printed soft actuators*. 2016. **250**: p. 258-272.
10. Chen, C.-T. and R.-C. Peng, *Design and 3D printing of paper-based shape memory polymer actuated for soft lightweight fingers*. *Smart Materials and Structures*, 2021. **30**(7): p. 075010.
11. Tawk, C. and G. Alici, *Finite element modeling in the design process of 3D printed pneumatic soft actuators and sensors*. *Robotics*, 2020. **9**(3): p. 52.
12. Zolfagharian, A., et al., *3D/4D-printed bending-type soft pneumatic actuators: Fabrication, modelling, and control*. *Virtual and Physical Prototyping*, 2020. **15**(4): p. 373-402.
13. Faller, L.-M., C. Stetco, and H. Zangl. *Design of a novel gripper system with 3D-and inkjet-printed multimodal sensors for automated grasping of a forestry robot*. in *2019 IEEE/RSJ International Conference on Intelligent Robots and Systems (IROS)*. 2019. IEEE.
14. Baniyadi, M., et al., *Constitutive Modeling of multi-stimuli-responsive shape memory polymers with multi-functional capabilities*. *International Journal of Mechanical Sciences*, 2021. **192**: p. 106082.
15. Pandini, S., et al., *Shape memory response and hierarchical motion capabilities of 4D printed auxetic structures*. *Mechanics Research Communications*, 2020. **103**: p. 103463.
16. Cheah, D.S., et al., *Development of 4D-printed shape memory polymer large-stroke XY micropositioning stages*. *Journal of Micromechanics and Microengineering*, 2022. **32**(6): p. 065006.
17. Miriyev, A., K. Stack, and H.J.N.c. Lipson, *Soft material for soft actuators*. 2017. **8**(1): p. 1-8.
18. Decroly, G., et al., *Optimization of Phase-Change Material–Elastomer Composite and Integration in Kirigami-Inspired Voxel-Based Actuators*. 2021. **8**: p. 113.

19. Hiremath, S., M. Shrishail, and S. Kulkarni, *Progression and characterization of polydimethylsiloxane-carbon black nanocomposites for photothermal actuator applications*. Sensors and Actuators A: Physical, 2021. **319**: p. 112522.
20. Xia, B., et al., *Improving the Actuation Speed and Multi-Cyclic Actuation Characteristics of Silicone/Ethanol Soft Actuators*. Actuators, 2020. **9**(3): p. 62.
21. Cartolano, M., et al., *Conductive Fabric Heaters for Heat-Activated Soft Actuators*. Actuators, 2019. **8**(1): p. 9.
22. Li, J., M. Sun, and Z.J.S.R. Wu, *Design and Fabrication of a Low-Cost Silicone and Water-Based Soft Actuator with a High Load-to-Weight Ratio*. 2020.
23. Qian, X., et al., *Untethered recyclable tubular actuators with versatile locomotion for soft continuum robots*. 2018. **30**(29): p. 1801103.
24. Han, J., et al., *Untethered soft actuators by liquid-vapor phase transition: remote and programmable actuation*. 2019. **1**(8): p. 1900109.
25. Garcia, M., et al. *Development of a 3D Printed Soft Parallel Robot*. in *ASME International Mechanical Engineering Congress and Exposition*. 2020. American Society of Mechanical Engineers.
26. Amiri Moghadam, A.A., et al., *Laser cutting as a rapid method for fabricating thin soft pneumatic actuators and robots*. Soft robotics, 2018. **5**(4): p. 443-451.
27. Juuti, J., M. Leinonen, and H. Jantunen, *Micropositioning*. 2008, Springer US. p. 319-340.
28. Al-Jodah, A., et al. *Design and Analysis of a Novel 3-DOF Large Range Micropositioning Mechanism*. IEEE.
29. Staicu, S., *Dynamics of a 3-PRR planar parallel robot*. UPB Scientific Bulletin, Series D: Mechanical Engineering, 2008. **70**: p. 3-18.
30. Decroly, G., et al., *Programmable Stimuli-Responsive Actuators for Complex Motions in Soft Robotics: Concept, Design and Challenges*. Actuators, 2020. **9**(4): p. 131.
31. Miriyev, A., et al., *Additive Manufacturing of Silicone Composites for Soft Actuation*. 3D Printing and Additive Manufacturing, 2019. **6**(6): p. 309-318.
32. Gogu, G., *Structural synthesis of parallel robots: part 3: topologies with planar motion of the moving platform*. Vol. 173. 2010; Springer Science & Business Media.
33. Singh, D., et al., *Workspace analysis of 3-DOF U-shape base planar parallel robotic motion stage using shape memory alloy restoration technique (SMART) linear actuators*. SN Applied Sciences, 2021. **3**(4): p. 1-22.
34. Singh, G. and G. Krishnan, *Designing fiber-reinforced soft actuators for planar curvilinear shape matching*. Soft robotics, 2020. **7**(1): p. 109-121.
35. Connolly, F., C.J. Walsh, and K. Bertoldi, *Automatic design of fiber-reinforced soft actuators for trajectory matching*. Proceedings of the National Academy of Sciences, 2017. **114**(1): p. 51-56.
36. Kapłon, T. and A. Milecki, *Linear Drive Based on Silicon/Ethanol Composite*. Polymers, 2021. **13**(16): p. 2668.
37. Miriyev, A., K. Stack, and H. Lipson, *Soft material for soft actuators*. Nature communications, 2017. **8**(1): p. 1-8.
38. Acer, M. and A. Şabanoviç, *Design, kinematic modeling and sliding mode control with sliding mode observer of a novel 3-PRR compliant mechanism*. Advanced Robotics, 2016. **30**(17-18): p. 1228-1242.
39. Zhang, H., et al., *Dynamic modeling and comparative analysis of a 3-PRR parallel robot with multiple lubricated joints*. International journal of mechanics and materials in design, 2020. **16**(3): p. 541-555.